ResearchGate

See discussions, stats, and author profiles for this publication at: https://www.researchgate.net/publication/374024498

# Surface rupture history and 18-ka-long slip rate along the Pazarcık segment of the East Anatolian Fault

**Article** *in* Journal of the Geological Society · September 2023

DOI: 10.1144/jgs2023-056

CITATIONS
4

READS
260

**2 authors:**



Önder Yönlü
FugroSial Geosciences, Consulting and Engineering, Turkey
**13** PUBLICATIONS **296** CITATIONS
SEE PROFILE



Volkan Karabacak
Eskisehir Osmangazi University
**113** PUBLICATIONS **1,614** CITATIONS
SEE PROFILE

All content following this page was uploaded by Volkan Karabacak on 07 January 2024.

The user has requested enhancement of the downloaded file.

Research article

JGS
Journal of the Geological Society

https://doi.org/10.1144/jgs2023-056 | Vol. 181 | 2023 | jgs2023-056

# Surface rupture history and 18 kyr long slip rate along the Pazarcık segment of the East Anatolian Fault

**Önder Yönlü[1] and Volkan Karabacak[2]***

[1] Fugro Geoservices Limited, Wallingford OX10 9RB, UK
[2] Department of Geological Engineering, Eskişehir Osmangazi University, 26040 Eskişehir, Turkey
VK, 0000-0003-2581-7984
* Correspondence: karabacak@ogu.edu.tr

**Abstract:** We investigate the palaeo earthquakes and slip rate on the Pazarcık segment of the East Anatolian Fault, which was involved in the surface rupture of the 6 February 2023 Pazarcık–Kahramanmaraş earthquake ($M_w$ 7.7) and provided insights into the long-term behaviour of this major continental fault. Palaeoseismological data from two trench sites reveal evidence for at least five surface ruptures in the Holocene Period. The historical earthquake of AD 1114 is verified at both trench sites but the following event of AD 1513 is identified at only one site. In addition, the age difference of the older events shows that historical activity is separated by much longer periods of relative quiescence that range from 500 to 1000 years, which suggests quasiperiodic earthquake occurrence on sub-segments of the Pazarcık segment. Our fault-parallel trenches revealed 101 ± 5 m offset in the last 18 kyr and 51 ± 1 m offset in the last 9 kyr on a buried stream channel and the actual channel of the same stream respectively. The correlation of the maximum and abandonment age of the channel with measured offsets revealed a 5.6 mm $a^{-1}$ long-term slip rate of the fault.

**Supplementary material:** A table and figures providing details of radiocarbon ages and trench sites are available at https://doi.org/10.6084/m9.figshare.c.6850786

**Received** 5 May 2023; **revised** 19 September 2023; **accepted** 19 September 2023

The left lateral East Anatolian Fault (EAF) is one of the major transform faults of the Eastern Mediterranean region (Fig. 1a). The fault extends for about 550 km between Karlıova and Türkoğlu where it meets the North Anatolian Fault (NAF) to the NE and the Dead Sea Fault to the SW (Fig. 1b). The northward motion of the Arabian Plate is taken up by the EAF, together with the NAF, accommodating the westward extrusion of the Anatolian Block. The EAF is often considered a continuation of the Dead Sea Fault to the north where differential motion of the Arabian Peninsula relative to the African plate occurs (Fig. 1a) (McKenzie 1972; Şengör *et al.* 1985). In the most recent comprehensive study Duman and Emre (2013) studied the fault and divided it into seven segments based on fault step-overs, jogs or changes in fault strike between Karlıova and the Amik Basin. There are different opinions on the location of the intersection between the Dead Sea Fault and the EAF; some researchers (e.g. McKenzie 1970, 1972; Dewey *et al.* 1973; Şengör 1980; Jackson and McKenzie 1984; Hempton 1987; Barka and Kadinsky-Cade 1988; Kempler and Garfunkel 1991; Westaway and Arger 1996; Koçyiğit and Erol 2001; Yönlü *et al.* 2017) have suggested Türkoğlu whereas others (e.g. Allen 1969; Arpat and Şaroğlu 1975; Şengör *et al.* 1985; Kelling *et al.* 1987; Şaroğlu *et al.* 1992; Över *et al.* 2004; Duman and Emre 2013) have considered the Amik Basin as the location. The left lateral Karasu Fault extends along the western margin of the Karasu Valley between the two proposed intersection areas (i.e. from Türkoğlu in the north to the Amik Basin in the south). The Karasu Fault, thus, is known to transfer a significant amount of slip between the EAF and the Dead Sea Fault, although there is still discussion on which fault system the Karasu Fault belongs to.

The EAF is known to have experienced several destructive earthquakes in historical time (Arvanitakis 1903; Sieberg 1932; Abdalyan 1935; Calvi 1941; Ben-Manahem 1979; Soysal *et al.* 1981; Ambraseys and Jackson 1998; Guidoboni and Comastri 2005). In 1114, a very large earthquake occurred somewhere in the Kahramanmaraş region whose magnitude is thought to be ≥7.8 (Ambraseys and Jackson 1998). Another large event occurred in 1513 and caused extensive damage in the cities of Tarsus and Malatya; based on the distribution and intensity of damage it is believed to have been of $M_s \geq 7.4$ (Ambraseys 1989). These earthquakes are attributed to reactivation of southwestern segments of the EAF, although the precise locations and magnitudes of these earthquakes are unclear owing to the lack of palaeoseismological studies. Apart from these two large historical events, no $M_s = 7.0$ or larger earthquakes occurred on the fault in the last century. This relative quiescence was ended on 6 February 2023 by the Pazarcık–Kahramanmaraş earthquake ($M_w = 7.7$), which resulted in a *c.* 300 km long multi-segment surface rupture across southeastern Türkey (Karabacak *et al.* 2023). The Erkenek and Pazarcık segments of the EAF and Karasu Fault were involved in the surface rupture, as well as a not previously mapped Narlı Fault (Fig. 1b).

The slip rate of the EAF was previously estimated as 9–10 ± 1 mm $a^{-1}$ by global positioning system (GPS) campaigns (Bertrand 2006; Reilinger *et al.* 2006; Aktuğ *et al.* 2016), 8–13 mm $a^{-1}$ by interferometric synthetic aperture radar (InSAR) studies (Walters 2013; Cavalié and Jónsson 2014), 4–11 mm $a^{-1}$ from geological data (Seymen and Aydın 1972; Arpat and Şaroğlu 1975; Kasapoğlu 1987; Westaway and Arger 1996; Çetin *et al.* 2003; Aksoy *et al.* 2007; Herece 2008), 6–19 mm $a^{-1}$ from plate kinematic analyses (Lyberis *et al.* 1992; Kiratzi 1993; Yürür and Chorowicz 1998) and 25–31 mm $a^{-1}$ from seismological data (Taymaz *et al.* 1991). However, the Late Holocene slip rate of the EAF was not accurately estimated owing to the lack of sufficient palaeoseismic data, and this determination is of critical importance for seismic hazard studies on adjacent faults.

In this study, we present results from palaeoseismic investigations along the 90 km long Pazarcık segment of the southwestern section

© 2023 The Author(s). Published by The Geological Society of London. All rights reserved. For permissions: http://www.geolsoc.org.uk/permissions. Publishing disclaimer: www.geolsoc.org.uk/pub_ethics

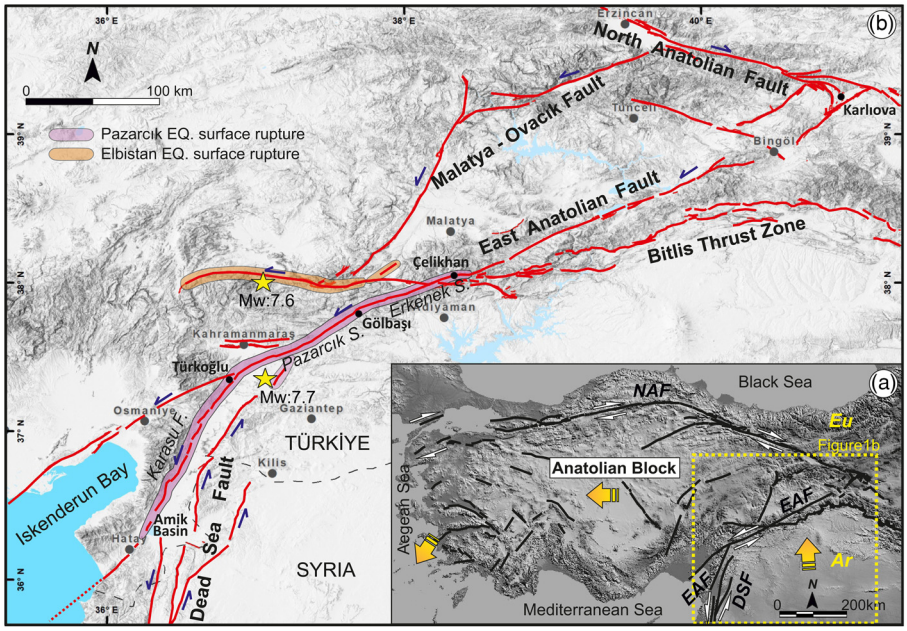



**Fig. 1.** (**a**) Main seismotectonic framework of the Eastern Mediterranean region with the movement of Arabia (Ar) and Anatolia relative to Eurasia (Eu). NAF, North Anatolian Fault; EAF, East Anatolian Fault; DSF, Dead Sea Fault. (**b**) Simplified map of the major active tectonic structures of East Anatolia, superimposed on shaded relief map derived from 30 m resolution Shuttle Radar Topography Mission (SRTM) data. Stars show the epicentres of the 6 February 2023 Pazarcık ($M_w = 7.7$) and Elbistan ($M_w = 7.6$) Kahramanmaraş earthquakes. Source: faults simplified and changed after Emre *et al.* (2013).

of the EAF. The age dating of palaeo-events and correlation with the historical data provide constraints on seismic slip history. In addition, mapping and age dating of an offset buried stream channel provides an 18 kyr long slip rate of the Pazarcık segment of the EAF. Finally, we discuss the earthquake behaviour of the segment, integrating palaeoseismological data and the coseismic displacements that occurred in the 2023 Pazarcık–Kahramanmaraş earthquake.

## East Anatolian Fault between Gölbaşı and Türkoğlu

The Pazarcık segment is the southernmost segment of the EAF before it intersects the Karasu Fault near Türkoğlu (Fig. 1b). The Pazarcık segment provides field evidence of sinistral displacement of stream beds by a few metres to kilometres, and faulted alluvial and colluvial deposits that extend for about 90 km between the Gölbaşı Basin in the NE and Türkoğlu in the SW (Fig. 2). Between Gölbaşı and Türkoğlu, the fault extends in pre-Quaternary rock units along most of its length. It cuts Quaternary deposits in limited areas in the Gölbaşı Basin to the NE and around Türkoğlu in the SW. The general morphology of the fault is characterized by linear topography and large cumulative offsets in river channels (Fig. 2). It can be traced by fault-related geomorphological features such as offset stream channels, elongated and shutter ridges, linear saddles, scarps and depressions that are aligned on a single trace. To the NE a left bend near Gölbaşı Lake forms the segment boundary between the Pazarcık and Erkenek segments (Fig. 2). The fault bounds the southeastern margin of the Gölbaşı Basin and caused a cumulative offset on the Aksu Stream of 16.5 km (Yönlü *et al.* 2013). Further SW of the Gölbaşı Basin, the fault extends in a high-relief area where three major stream channels, from south to north the Kısık, Koca and Gök streams, have recorded left lateral offsets of 4.4, 4.5 and 6.4 km, respectively (Fig. 2). Besides these large cumulative offsets, the majority of the stream channels show some evidence of left lateral offset on the fault trace. Near Kartal village, the fault makes a 1.5 km wide right bend, which causes uplift of the southern block owing to local transpression (Fig. 2). Based on the Kartal restraining bend, the Pazarcık segment can be separated into two geometrical sub-sections, namely the Gölbaşı and Tevekkelli sub-sections (Fig. 2). It forms the contact of Cretaceous Neotethyan ophiolite and Quaternary alluvium between the towns of Çiğli and Küpelikız and follows the SE-facing escarpment. This is one of the areas where the fault disrupts the Quaternary deposits. Left laterally displaced stream channels in the Holocene sediments indicate the recent activity of the fault. Further SW, elongated ridges, offset stream beds and shutter ridges are the geomorphological evidence of active faulting. The morphological expression of the fault diminishes to the east of Türkoğlu where it enters the Aksu River alluvial plain (Fig. 2).

The surface rupture of the 6 February 2023, $M_w = 7.7$, Pazarcık–Kahramanmaraş earthquake reveals the fault location, which is mostly in line with our fault mapping based on geological and geomorphological field observations (Fig. 2). During this earthquake, the entire length of the Pazarcık and Erkenek segments of the EAF and the Karasu Fault were reactivated (about 300 km), and an average of 3.0 m and maximum 7.3 m coseismic displacement occurred (Karabacak *et al.* 2023). The surface rupture revealed the fault location at the Aksu River plain near Türkoğlu where it intersects with the Karasu Fault. The surface rupture splays into two near Küpelikız village; the northern rupture continues with the same trend towards Türkoğlu and the southern rupture makes a 20° bend towards the south and extends along the Karasu Fault (Fig. 2). Although the rupture extends about 1.3 km SW of Küpelikız towards Türkoğlu (Fig. 2), it did not break the Imalı segment of the EAF.

In addition, a surface rupture of at least 10 km in length (Fig. 2) with a 3.2 m maximum left lateral offset was developed on the Narlı Fault to the south of the Pazarcık segment in the Aksu Basin (Karabacak *et al.* 2023). The N20E-trending rupture extends transverse to the Pazarcık segment and almost parallel to the Karasu Fault. The surface rupture on the Narlı Fault does not extend to the EAF in the north but the distribution of aftershocks suggests that the rupture connects with the EAF at depth around the Nacar step-over. Karabacak *et al.* (2023) stated that there is an increase in the amount of left lateral offset towards the NE along the surface rupture.

## Palaeoseismological trenching

To retrieve the chronology of historical earthquakes that ruptured the surface on the Pazarcık segment, we excavated trenches at two sites in 2010 and 2011. Our trench sites are located near the NE and SW ends of the Pazarcık segment (Fig. 2). Our trenching attempts in a small depression near Kartal village in the middle of the segment did not provide sufficient information because of the thick, chaotic bedded, coarse sediments encountered in the trench. In our successful trench locations in the Gölbaşı Basin to the NE and at Tevekkelli to the SW, the Pazarcık–Kahramanmaraş 2023 earthquake ruptured the surface as a single line, indicating successful trench location selection.

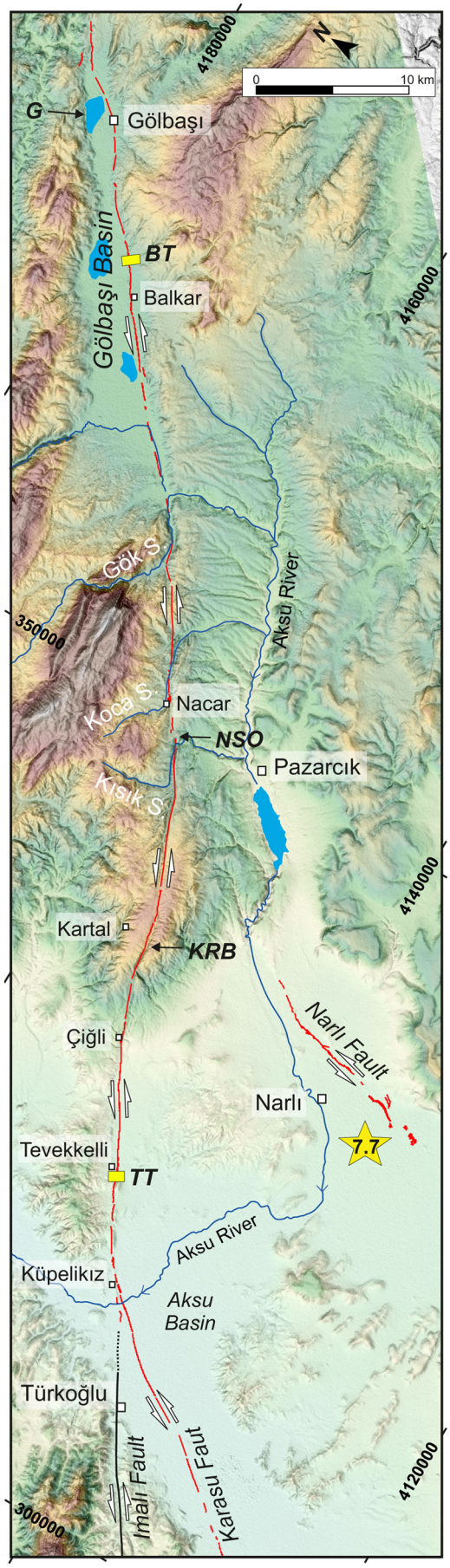



**Fig. 2.** Shaded relief map (30 m resolution SRTM data) of the EAF between Gölbaşı and Türkoğlu, showing the surface rupture (red line) of the 6 February ($M_w$ = 7.7) Pazarcık–Kahramanmaraş earthquake (yellow boxes are the trench sites). G, Gölbaşı Lake; NSO, Nacar releasing step-over; KRB, Kartal restraining bend; BT, Balkar trench site; TT, Tevekkelli trench site.

The trenches were excavated in areas where slow but continuous sedimentation is anticipated to allow an older rupture history to be captured at relatively shallow depths (Supplementary material Figs S1 and S2). Following excavation, the trench walls were cleaned by hand tools. Metre marks were established on the trench wall by measuring nail locations with a tape measure in the field along level lines. The trench photographs were taken to provide a minimum of 60% vertical and horizontal overlap and they were processed using Agisoft Photoscan® to develop full trench wall photomosaics, and all observations are mapped on the print-outs at 1/10 scale. Charcoal and bulk samples collected from our trenches were analysed by accelerating mass spectrometry (AMS) at the Poznan Laboratory, Adam Mickiewicz University. In our description of unit ages below, we used OxCal v4.4.4 (Bronk Ramsey 2017) with an Intcal13 calibration curve (Reimer *et al.* 2013) to determine the calibrated calendar ages (Supplementary material Table S1).

## Balkar trench site

The Balkar trench site is located in the Gölbaşı Basin to the NE (Fig. 2). In this area the fault is characterized by pressure ridges, shutter ridges and left lateral offset stream beds indicating long-term activity. Our trench site lies to the NE of a fault-parallel elongated ridge, on farm fields gently sloping towards the NW (Fig. 3a).

In this area, the near-surface sediments derived from highlands to the east are transported by ephemeral channels, which probably are active only during significant rainfall and control the accumulation of fine-grained material in alluvial fans on gentle topography. We excavated two trenches about 270 m apart and both were cut by the surface rupture of the Pazarcık–Kahramanmaraş 2023 earthquake (Fig. 3a and Supplementary material Fig. S2). Trench T1 exposed a deformation zone a couple of metres wide with several discrete fault planes deforming coarse-grained deposits (Supplementary Fig. S3). Unfortunately, the number of age-dating samples retrieved has been not enough to allow us to discuss the earthquake history at this specific site. Therefore, a second trench was dug to the north, which exposed fault planes in a succession of fine-grained sediments.

The 20 m long, 3 m deep, trench T2 (374 151 m E/4 177 773 m N) was excavated perpendicular to the EAF trace (Fig. 3a). Both walls were cleaned, photographed and logged in detail. Because both walls yield similar information in terms of lithology and palaeo-events, we present only the SW wall log (Fig. 4). The first 13 m of the trench log is presented here as there are no lithological changes or fault-related deformation observed in the remaining section of the trench.

The trench exposed highly to completely weathered bedrock comprising finely to coarsely interbedded mudstones, claystones, siltstones and sandstones overlain by predominantly clay and silt-rich alluvium or colluvium deposited on a gentle slope. Some of the clay units have a high organic matter content and include thin peat horizons. The stratigraphic contacts between clay-rich and silt-rich layers were distinguished with the help of desiccation cracks within the clay units. The scattered fine- to medium-sized gravel and the presence of rare cobbles within clay units indicate a low-energy gravitational depositional environment. Descriptions of each unit are presented on the trench log (Fig. 4).

The fault in the trench was identified by the sharp colour differences between bedrock, fault gouge and alluvial units. The highly weathered bedrock unit is imposed above the sedimentary units along a 45°SE-dipping fault plane. The position of the fault plane indicates that the motion on the fault is strike-slip with some reverse (SE-side-up) component. The compressional deformation can be seen in the sudden reversal of bedding dip direction from SW to NE on either side of the fault.

At meterage 3 of the trench wall, there is a *c.* 10 cm thick, silty very fine sand (unit 25) identified subvertically along the fault at the

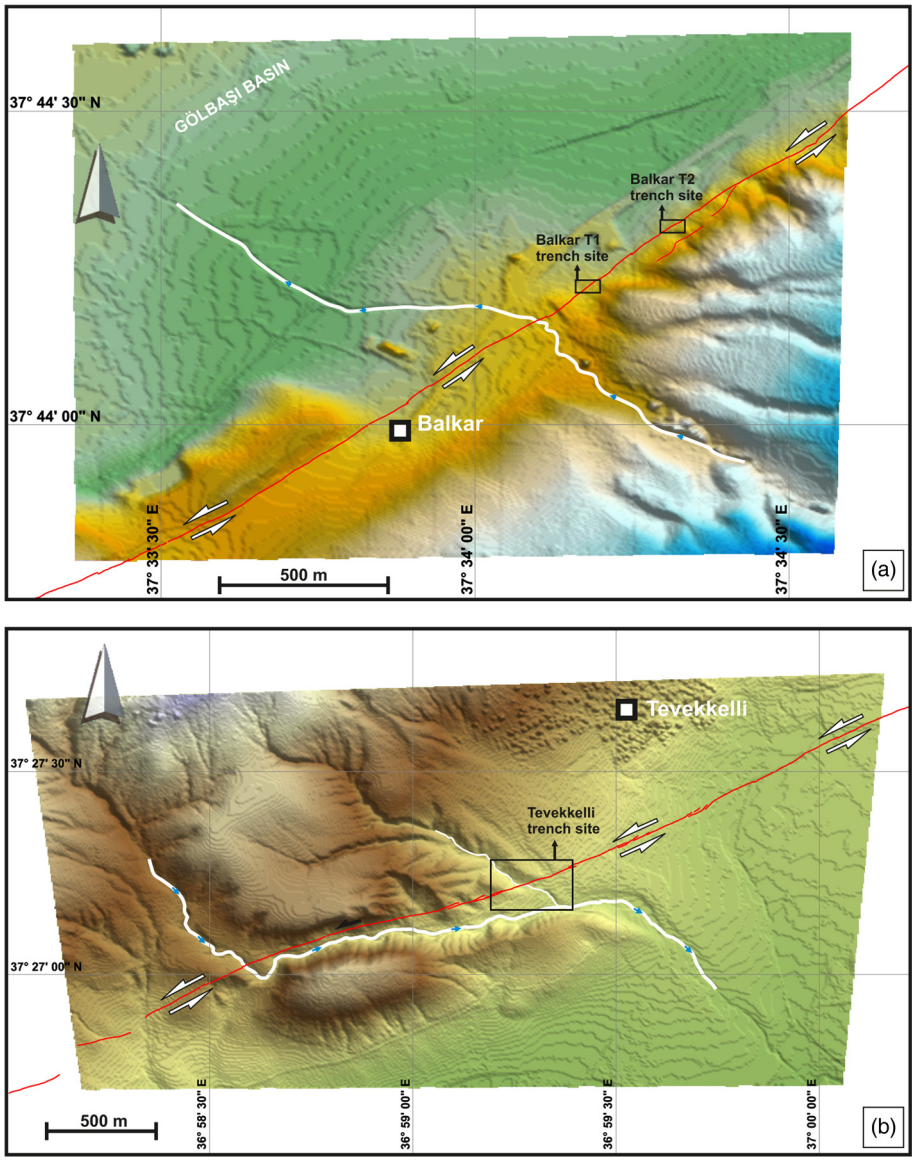



**Fig. 3.** (**a**) Shaded relief map of Balkar trench site. (**b**) Shaded relief map of Tevekkelli trench site. Red line shows the surface rupture of the 6 February (Mw = 7.7) Pazarcık–Kahramanmaraş earthquake; white lines show the rivers. For (**a**) and (**b**) the digital elevation model with a resolution of 5 m was generated using aerial stereo pairs.

interface of bedrock and alluvial units. It extends upward from the bottom of the trench and terminates at 1.5 m below the ground. The composition and subvertical position of the unit may indicate a palaeo-liquefaction, related to strong ground shaking by one of the historical earthquakes.

## Faulting at the Balkar trench

The faulting is confined to a 1 m wide zone at the SE end of the trench. The repeated surface ruptures caused intense deformation along this narrow zone. Owing to numerous movements in the same narrow zone the traces of the past surface ruptures overlapped each other, making it impossible to distinguish different earthquake records. The trace of the most recent earthquake extended up to the base of the present soil (Fig. 4).

The evidence of the penultimate event (event Y) is identified by the sudden termination of units 24 and 22 at trench chainage (distance from the end of the trench) 3.5 m. The fault plane of this event reaches up to the base of the present soil. Historical data, however, do not suggest a recent historical earthquake in this area. Considering the position and geometry of the preceding unit of the present soil, the event is constrained by unit 23. The tiny vertical crack with fine sand infill at chainage 9.8 m may be related to the same event and it clearly terminates below unit 23. Age dating of a charcoal sample indicates that the lower boundary age of the unit is AD 990–1390. This event (event Y) can be correlated with the 1114 earthquake (Mercalli Intensity Scale $I_0$ = VIII–X), which caused heavy damage in the Kahramanmaraş and Adıyaman regions (Arvanitakis 1903; Sieberg 1932; Soysal *et al.* 1981; Ambraseys and Jackson 1998; Guidoboni and Comastri 2005).

The deformation related to the antepenultimate event (event X) bounds unit 21 to the SE and does not cut through unit 22. No radiocarbon sample was found to cap the event; however, it is likely that it occurred after the deposition of unit 22, which is dated to 811–401 BC. The very similar age of the charcoal sample taken in the fault gauge indicates that some portion of unit 20 was mixed into the fault gauge by shearing during surface faulting. No other discrete fault splays were identified in the trench to allow evaluation of the previous events by a 'cut and bury' relationship. However, the two organic clay-rich layers units 13 and 14 overlain by colluvial deposits in the lowermost part of the trench wall can be related to historical earthquakes. The SE dip of units 11 and 12 indicates that fault deformation caused tilting. We infer that back-tilting against the topography caused a depression and probably surface water ponding for some time. As a result, organic-rich clay was deposited in the depression, and it was later overlain by colluvial deposits. According to this interpretation, units 13 and 16 predate two past earthquakes, which can be constrained by four radiocarbon dates. The oldest identified event in the trench is dated between 2811 and 2391 BC and the following earthquake occurred between 1781 and 1221 BC.

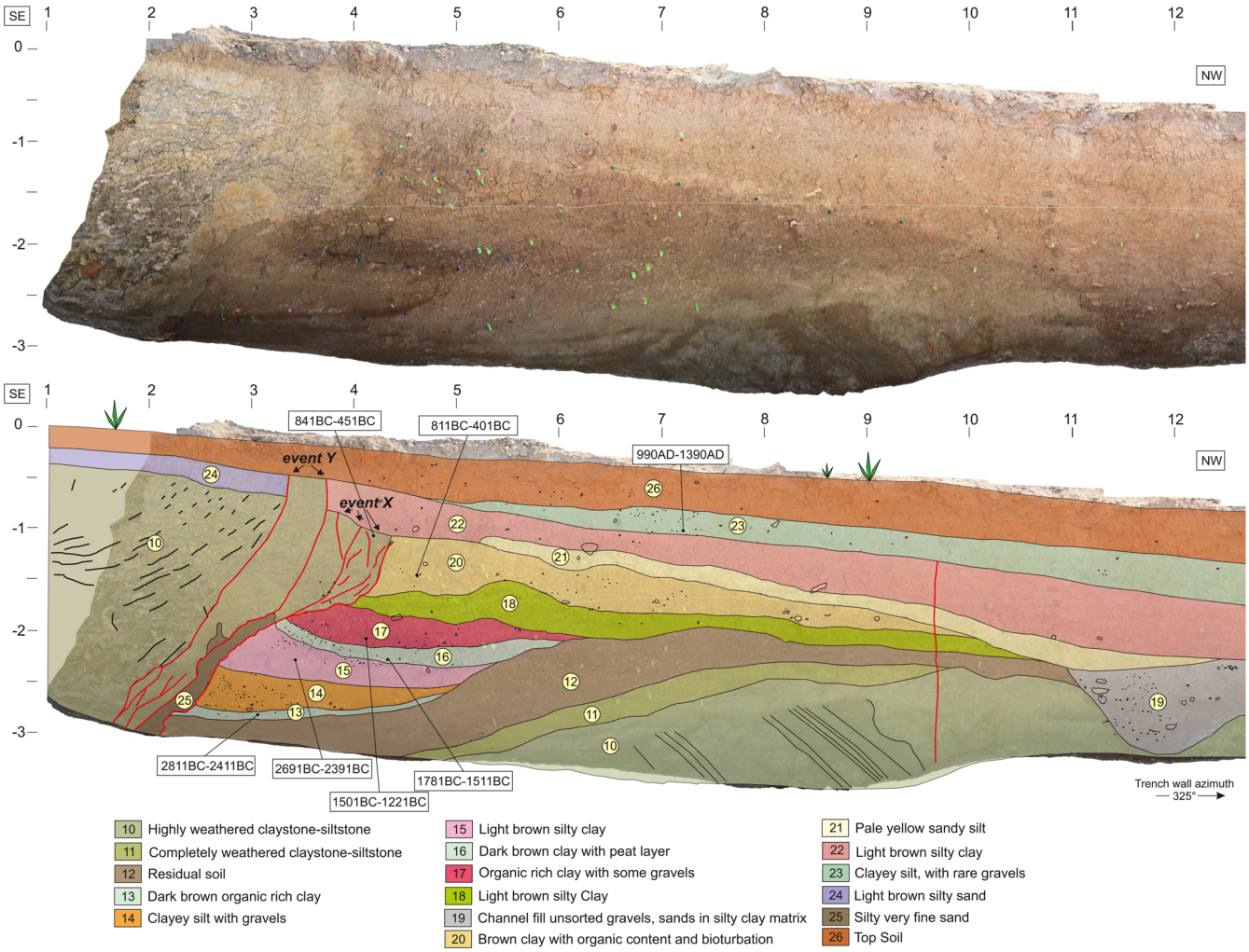



**Fig. 4.** Photomosaic (**a**) and trench log (**b**) of SW wall of Balkar trench. Thin black lines are stratigraphic contacts, colours show units, red lines are traces of faults and small rounded outlines are gravels (trench location 374 154 m E/417 775 m N).

## Tevekkelli trench site

The Tevekkeli trench site is located in the southwestern part of the Pazarcık segment between Kocalar and Tevekkeli villages (Fig. 2), about 10 km NE of Türkoğlu. The EAF at this site is expressed as a single, geomorphologically well-defined strand. It is characterized by left laterally displaced stream channels and fault scarps, juxtaposing different rock units in the area. The cumulative 1.3 ± 0.2 km offset on an ephemeral stream (Fig. 3b and Supplementary material Fig. S1) indicates the long-term slip that developed on the fault at this locality. The offset stream geometry and linear shutter ridge in the area show that the fault motion occurs in a narrow zone, as shown by the 2023 surface rupture (Fig. 3b). Our fault mapping prior to the earthquake and the surface rupture mapping after the 2023 event support the view that the fault constitutes a single trace without additional secondary splays (Fig. 3b).

The trench site is located on a low-relief southward sloping pediment at 565–570 m asl (above sea level). The site is bounded to the north by relatively high topography and to the south by a fault-parallel stream valley and a shutter ridge (Supplementary Fig. S1). The fine and coarse sediment supply to the site comes from higher land to the north and is deposited as alluvium across the trench site. The deposits in riverbeds are characterized by sands and gravels whereas they are mostly clays, silts and sands on adjacent areas of low relief. A total of four trenches were excavated in the alluvial deposits near a seasonal stream that shows a prominent left lateral offset (Fig. 5). Following the identification of the EAF in trench T1, the trench C1 was dug a few metres to the east to identify any buried channel at shallow depth. Once channel fill was exposed in C1, C2 was excavated a few metres to the east oblique to the fault to maximize the chance to observe the continuation of the same buried channel. Finally, the last trench, C3, was opened to the south of the asphalt road as there is no alternative trench location and the buried channel was also exposed in this trench. The coordinates of the fault in T1 as well as the thalweg and edges of the buried channels in trenches C1, C2 and C3 were taken by total station. The excavations yielded valuable information about earthquake history and slip rate, and data from these trenches are presented here.

## Faulting at the Tevekkelli trench

T1 is a fault-perpendicular trench excavated for accurate fault location and investigation of surface-rupturing events (Fig. 5). The 20 m long by 3 m deep trench was dug where a prominent narrow lineament and a low-relief scarp are present. It revealed well-stratified sedimentary units cut by discrete shear planes (Fig. 6).

The trench exposed a prominent shear zone consisting of variably coloured, pervasively sheared plastic clay gouge (Fig. 6). Dominant strike-slip movements are indicated by the clear sets of shear fabric aligned along the different faults and by the presence of detached faulted blocks and sheared material in the fault core. The shear zone dips at an angle of 60–65° to the NW. Owing to the high dip angle some amount of dip-slip movement was expected; however, there was no clear vertical offset observed on the 2023 earthquake surface rupture. Intense fault deformation is inferred from the different sets

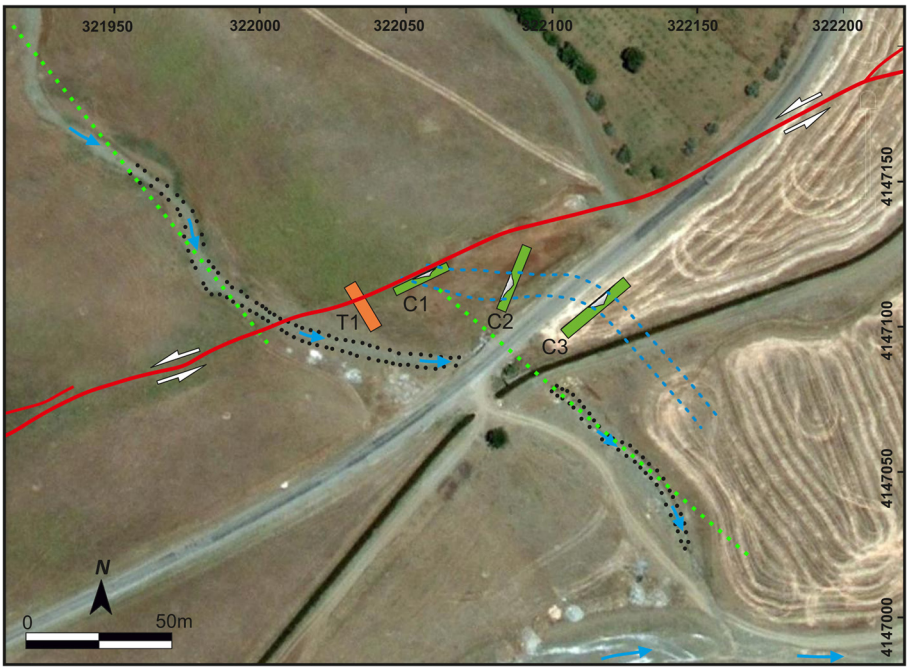



**Fig. 5.** Satellite image of Tevekkelli trench site, showing trench locations and offset measurements before the 6 February ($M_w$ = 7.7) Pazarcık–Kahramanmaraş earthquake. Black dots are the survey locations of the actual stream bed with D-GPS, blue dashed lines are the inferred position of the buried stream channel based on the trench data, green dashed line is the offset measurement reference line for the actual stream and orange dashed line is the offset measurement reference line for the buried stream channel. Location 37°27'13.00"N, 36°59'16.44"E, eye altitude 780 m. Sources: base maps were taken from Google Earth software V 7.3.6.9345 (06/15/2010), DigitalGlobe 2010, http://www.earth.google.com.

of shear fabric, which are aligned along the different shear zones in relation to the corresponding capping layers. As the shear fabric is characteristic of coseismic movement, the set of palaeo-earthquakes were inferred to be surface rupture events with large magnitudes. The fault core is about 30 cm wide at the bottom of the trench and it broadens upward to about 100 cm associated with fault splays.

There were clear mismatches in individual units across the fault, with relatively older units sited on its northern side (Fig. 6). We interpret this as the consequence of substantial lateral slip at the site. We found evidence of five different surface ruptures in the Tevekkelli T1 based on upward fault terminations. The penultimate surface rupture on the trench walls is defined by two fault strands that terminate upward just below the topsoil. Unit j is thicker on the southeastern block of the fault. The fault strand was constrained by the topsoil and unit j, which have yielded radiocarbon ages of AD 1515–1845 and AD 1430–1680, respectively. Taking into account historical catalogues, the only recorded large event after the 15th century in this region is the 1513 earthquake ($I_0$ = VIII), which caused heavy damage across a wide area between Malatya and Kilikya (Calvi 1941; Soysal *et al.* 1981; Ambraseys 1989). Based on the correlation of radiocarbon dating and the historical accounts, the 1513 event is the penultimate event (event Y) in our trench. The previous event in the trench was identified by upward termination of two fault strands by unit j. Radiocarbon dating yielded a lower bound age of AD 1240–1470. This event (event X) can be correlated with the 1114 earthquake ($I_0$ = VIII–X), which is also evident in the Balkar trench. The older event (event V) is predated by unit h and has given an age of 3321–2871 BC. Given the age of unit h, more events could be expected between event V and event X, but evidence of this could not be identified in the trench, most probably because of overwriting surface ruptures. There are at least two further older events cutting unit f, which has yielded an age of 5961–5631 BC and is predated by unit h. However, the trench stratigraphy does not allow us to differentiate these events. The oldest event in the trench was identified as a fault splay that terminates below unit d. Two radiocarbon ages from unit d and the last cut unit c suggest that the oldest event in the trench occurred between 7561–7131 and 8591–7961 BC. The overall evaluation of the trench data and the expected recurrence interval of surface rupturing events on the EAF based on the historical records and GPS slip rates suggest that some of the historical events were missed in the trench. The most likely reason for this is that fault rupture was confined to the same zone in each earthquake and subsequent events overwrote the traces of the previous fault strands.

The uppermost stratum, unit k, is the modern 'A horizon' and contains abundant roots and organic debris. It is slightly thicker on the southern block of the fault, possibly related to the fault scarp of the last surface rupturing event.

The radiocarbon dates indicate that the section exposed in T1 is Early to Late Holocene in age. Nine detrital charcoal age determinations from Trench T1 are in stratigraphic order, suggesting minimal reworking. The fact that almost 10 000 years of the section is presented in less than 2 m of strata in the trench is probably a result of very low sedimentation rates.

## Tevekkelli fault-parallel trenches: channel offset and cumulative slip

The stream in this trench area flows across the fault zone on relatively flat topography (Fig. 5). The width of the stream bed varies between 3 and 6 m, and the active channel is about 1–2 m wide. The active channel bed comprises gravel and sand, transported from the elevated ground to the north. The channel was surveyed by differential (D-)GPS in 2011 and the left lateral offset on the channel was recorded as 48 ± 1 m (Fig. 5). It should be noted that Karabacak *et al.* (2023) measured 3 m of left lateral coseismic offsets near this area after the 2023 Pazarcık–Kahramanmaraş earthquake, thus the total offset on the channel is 51 m at present. Actual channel geometry and total offset indicate that the stream channel has followed the same route for a long time. However, although it is difficult to generate new channel incisions in a flat topography following slip on the fault, a semi-flat topography favours the formation of at least one new stream channel.

Considering the stream flow direction and strike-slip movement on the fault, we excavated Trench C1 near the eastern side of the stream on the southern block (Fig. 5 and Supplementary material Fig. S4a). The C1 trench exposed an asymmetrical buried channel 5 m wide and 1.5 m deep incised into reddish-brown stiff clay (Fig. 7a). The channel infill consists of gravels and sands with clay pockets. The steeper channel geometry of the northeastern side shows that the stream was curved towards the east, which is consistent with the fault motion. The imbrication of gravel clasts

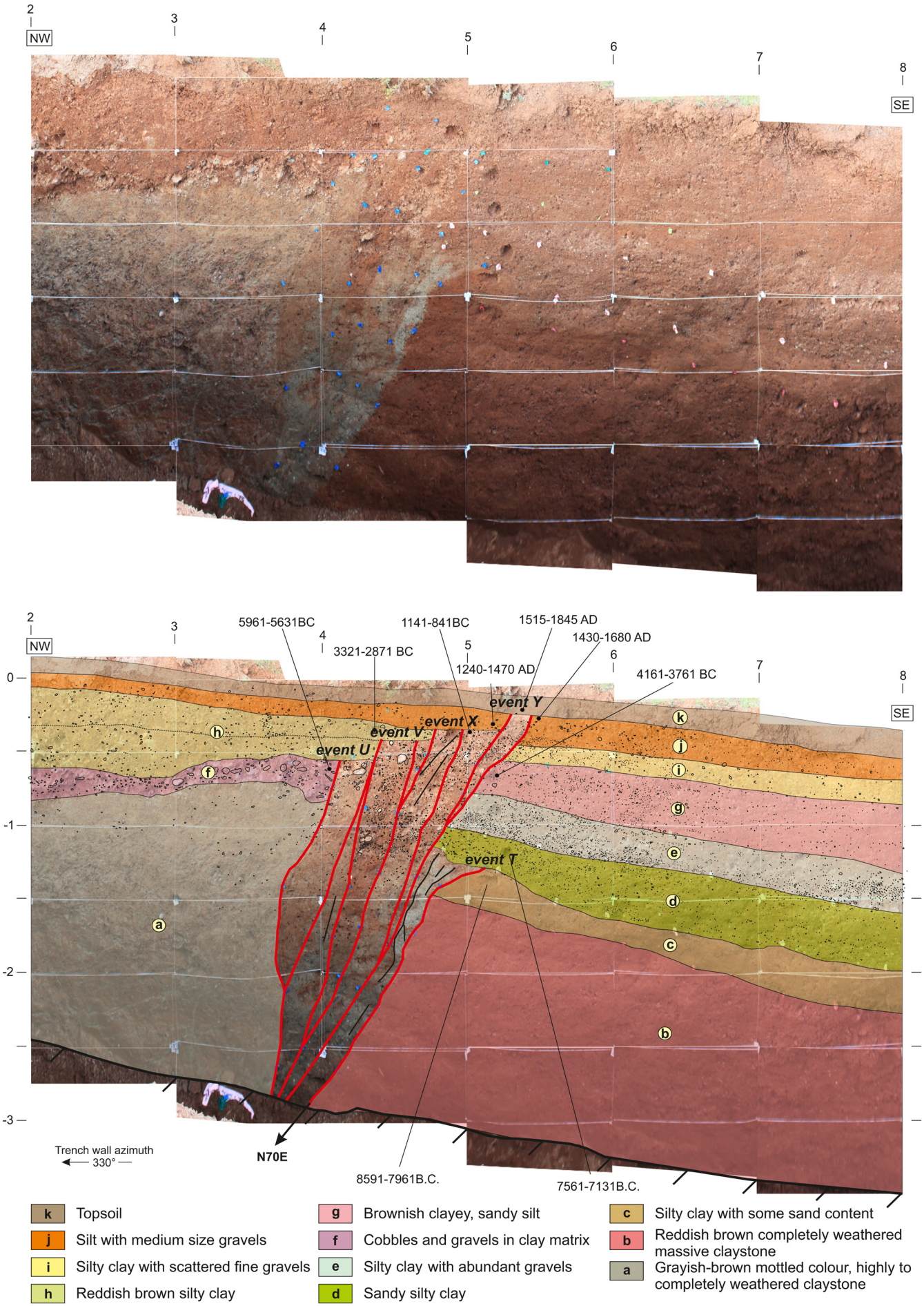



**Fig. 6.** Photomosaic (**a**) and trench log (**b**) of NE wall of Tevekkelli trench. Thin black lines are stratigraphic contacts, colours show units, red lines are traces of faults and small rounded outlines are gravels (trench location 322 045 m E/4 147 107 m N).

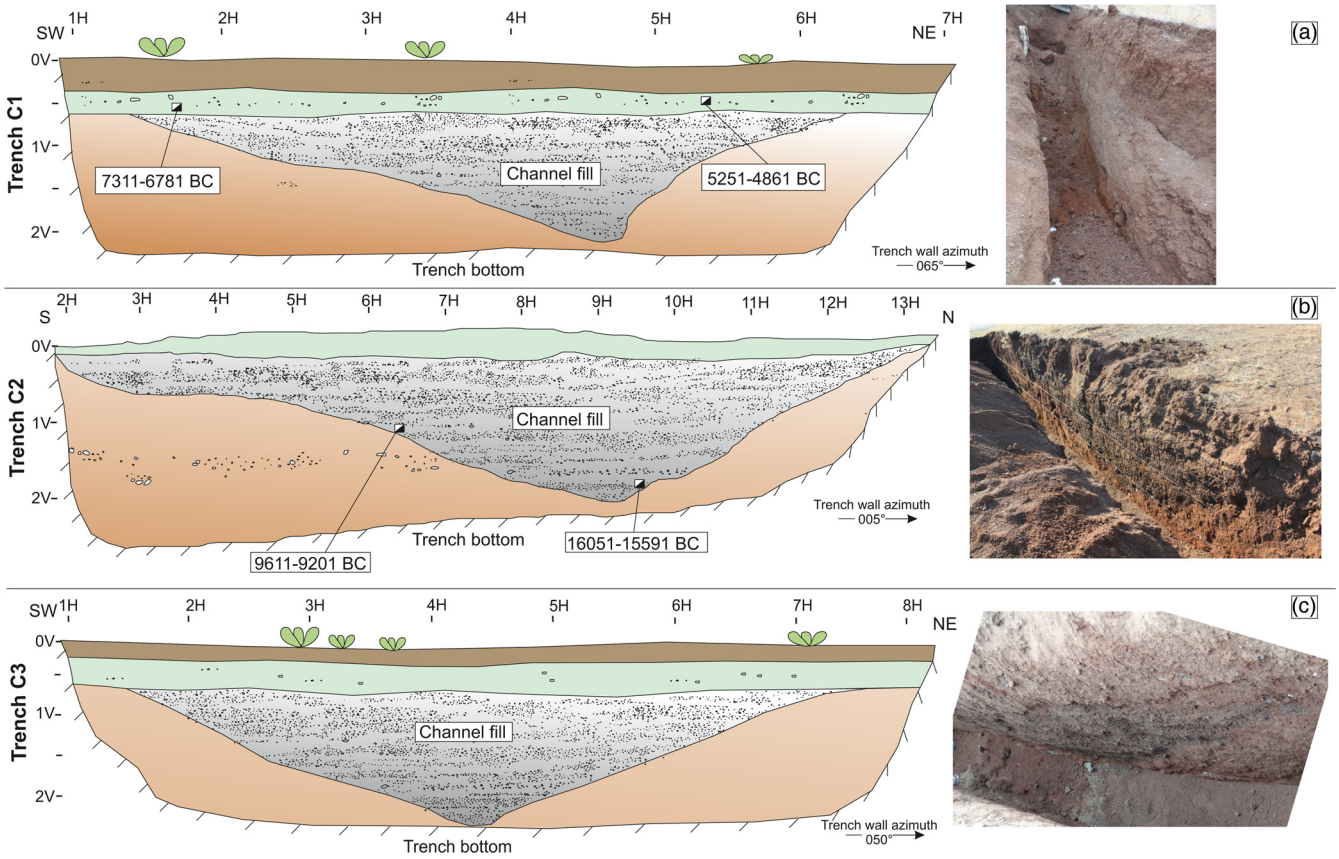



**Fig. 7.** Trench logs and photographs of buried stream channels identified at Tevekkelli trench site on the southeastern block of the EAF: (**a**) Trench C1; (**b**) Trench C2; (**c**) Trench C3. Thin black lines are stratigraphic contacts, colours show units and rounded black outlines are gravels.

indicates that the flow direction was towards the ESE. To trace the abandoned stream channel Trench C2 was excavated downstream of Trench C1 (Fig. 5). A similar asymmetrical buried channel was exposed in the trench (Fig. 7b and Supplementary Fig. S4b). As a result of previous soil stripping in that location by local farmers, topsoil was not preserved in Trench C2. The channel fill was 10 m wide and the northern side was steeper, similar to the channel in Trench C1. A further trench, C3, was dug SE of Trench C2 to examine the morphology of the buried channel stream further downstream (Fig. 5). In this third trench, a symmetrical channel geometry was observed (Fig. 7c), which indicates the buried channel extending towards the SE, more or less parallel to the actual stream channel.

All trench walls were gridded and studied but detailed logging was performed only in one wall and selected wall sections that exposed buried channel features. All trenches encountered similar fluvial sediments infilling the channel incised into the same stiff clay (Fig. 7). The V-shape of the buried channels allowed precise mapping of the thalwegs. The thalwegs and margins of the buried channels were surveyed by D-GPS (see dashed lines in Fig. 5) to allow comparison with the active stream channel on the northern block of the fault. The left lateral cumulative offset on the buried channel was measured as 98 ± 5 m (Fig. 4) in 2011, before the 6 February 2023 Pazarcık–Kahramanmaraş earthquake.

Bulk samples of the clay lenses within the channel infill close to the thalweg were collected from Trenches C1 and C2. Although it is possible that the carbon in these samples may have been transported from upstream, it is reasonable to conclude that age dating will provide the maximum age of the channel fill. The lowermost sample yielded 16 051–15 591 BC whereas the sample above yielded a consistent age of 9611–9201 BC. The channel infill was overlain by the same colluvial unit in all three trenches. To obtain the abandonment age of the channel, two radiocarbon dating samples were collected from the colluvium. Analysis yielded dates of 7311–6781 and 5251–4861 BC. As a result of soil barrowing by the farmers at the C2 trench site, we hesitated to collect samples from the uppermost part of the trench as there is a possibility of disturbance. However, as we were able to identify the same channel in all trenches, it is safe to use the dates from different trenches to understand the deposition and abandonment.

## Discussion

### Correlation of palaeo events

Our trenches at the Balkar and Tevekkelli sites provided evidence of repeated surface rupturing events on the Pazarcık segment of the EAF. In addition to the 1513 and 1114 earthquakes, we found evidence of at least three, or possibly more, earlier surface ruptures during the past 10 000 years. The historical 1513 earthquake has been identified in the Tevekkelli trench but not in the Balkar trench in the Gölbaşı Basin. This may suggest two possible scenarios.

(1) The 1513 earthquake ruptured through the Gölbaşı Basin but the event horizon is missed in the Balkar trench owing to erosion or lack of sedimentation at the trench location after the earthquake. However, we have not identified an erosion surface on the uppermost units exposed in the trench.

(2) The 1513 earthquake occurred on the EAF further SW, ruptured only a part of the system and the rupture cut through Tevekkelli trench site, but the northeastern extent of the rupture is terminated somewhere before it reached the Gölbaşı Basin. This requires an irregularity in the fault geometry such as large step-over or bend that is capable of

terminating the surface rupture. Our fault mapping based on the geological and geomorphological evidence shows only the Kartal restraining bend as a major geometric irregularity on the Pazarcık segment that may have caused termination of the previous surface ruptures. The increase in offsets of up to 7.3 m caused by the 6 February 2023 earthquake to the NE of Nacar village (Karabacak *et al.* 2023) suggests that more stress has accumulated in the northeastern part of the fault segment, and most probably this part of the fault has not been ruptured for a longer duration than the Tevekkelli sub-segment.

Our findings imply that the 1513 earthquake surface rupture does not extend NE of the Kartal restraining bend; however, the southwestern extent of this historical event is unknown, and more palaeoseismological trenching is required to the SE of Türkoğlu on both the Imalı and the Karasu segments. Based on the damage distribution, the event should be $M > 7$, so this earthquake may have produced a surface rupture at least 100 km long. The surface rupture may have advanced along the Karasu valley, as in the 2023 Pazarcık–Kahramanmaraş earthquake, or it may have passed to the west of Türkoğlu and ruptured the Imalı Fault segment in the Amanos Mountains. Considering that the Imalı Fault was not ruptured by the 6 February 2023 earthquake, we assume that the 1513 earthquake ruptured through the Imalı Fault.

The evidence for the historical 1114 earthquake was identified in both trenches, which indicates that the entire length of the Pazarcık segment has been ruptured, as a minimum. According to the intensity distributions and extensive damage in a wide area reported by historical accounts, the 1114 earthquake was one of the greatest events in this area. Therefore, it can be considered that the 1114 earthquake generated a similar length rupture to the 6 February 2023 Pazarcık–Kahramanmaraş earthquake.

Although several older events were identified in our trenches and constrained by AMS dating, the lack of published palaeoseismological data along the Pazarcık segment and historical earthquake records limited to two major earthquakes for this area do not allow us to precisely correlate the previous events. On the other hand, the age dating of these events falling into different time brackets suggests that the Tevekkeli and Gölbaşı sub-segments ruptured at different times in the past. It can be interpreted that the Kartal restraining bend played an important role in rupture propagation in the past. The fact that the age dating of events in our trenches falls into different time intervals suggests that the earthquake occurrence is quasiperiodic, with relatively larger earthquakes ($M > 7.5$) of multi-segment ruptures occurring with *c.* 1000 year recurrence periods and sub-segments generating $M \asymp 7$ earthquakes at nonuniform intervals. Other major fast slipping transform faults also have bimodal behaviour (i.e. San Andreas Fault, Zielke *et al.* 2010; Alpine Fault, De Pascale *et al.* 2014; North Anatolian Fault, Karabacak *et al.* 2019). Because the dating of the palaeo events reflects multiple rupture behaviours along the EAF segments, it can be seen that the EAF has a similar bimodal behaviour to the San Andreas, Alpine and North Anatolian faults.

## Slip rate estimation

Our three fault-parallel trenches on an abandoned and displaced stream channel have provided the first palaeoseismological slip rate estimate for the Pazarcık segment of the EAF. According to the age dating of buried stream deposits and the cumulative slip measured on the actual and abandoned stream channels, we measured $98 \pm 5$ and $48 \pm 1$ m offsets accumulated over a period of 17 800 and 9000 years, respectively. Considering the slip of the 6 February 2023 Pazarcık–Kahramanmaraş earthquake on top of the cumulative offsets measured in 2011 (Karabacak *et al.* 2023), 3 m offset was added to the cumulative slip after the earthquake. Therefore, the cumulative offset on the abandoned and actual stream is $101 \pm 5$ and $51 \pm 1$ m after the earthquake. The offset amounts and age dating revealed $5.6 \pm 0.3$ mm $a^{-1}$ slip of the fault (Fig. 8). The fact that the slip rate for two different long periods is the same can be interpreted as indicating no significant change in the slip rate of the fault in the last 18 kyr.

Our palaeoseismological slip rate data fit with the lower bound of the 4–11 mm $a^{-1}$ slip rate on the EAF estimated from offset geological markers (Seymen and Aydın 1972; Arpat and Şaroğlu 1975; Kasapoğlu 1987; Westaway and Arger 1996; Çetin *et al.* 2003; Aksoy *et al.* 2007; Herece 2008). In addition, these data are consistent with the slip rate estimates of *c.* 4–4.5 mm $a^{-1}$ based on the offset geological markers (Rojay *et al.* 2001; Karabacak 2007; Seyrek *et al.* 2007) on the Karasu Fault and 5–6 mm $a^{-1}$ archaeo- and palaeoseismological slip rate estimates on the northernmost Dead Sea Fault (i.e. Hacıpaşa Fault) (Altunel *et al.* 2009; Yönlü *et al.* 2010) (Fig. 8). However, it is considerably lower than the most recent GPS slip rate estimate of $10.3 \pm 0.6$ mm $a^{-1}$ (Aktuğ *et al.* 2016). This suggests that the GPS slip rate is not applicable to the long term, and it may be higher than the geological slip rate owing to post-seismic relaxation or deformation that is not accommodated by the EAF because GPS data are collected at a significant distance from the fault. Furthermore, the 2023 Pazarcık–Kahramanmaraş earthquake demonstrated that some of the slip accommodated by the Narlı Fault also transferred to the EAF somewhere near Nacar village. Our Tevekkelli trench site where we obtained the slip rate data is located SW of this location. Therefore, a higher slip rate should be expected on the EAF to the NE of the Narlı Fault intersection. There are no slip rate data on the Narlı Fault yet; however, comparing the morphological trace and geometry of faults, the Karasu Fault presents a more prominent morphology with offset streams, shutter ridges, etc. than the Narlı Fault. This allows us to infer that the Karasu Fault accommodated relatively higher slip rates with shorter recurrence intervals than the Narlı Fault, therefore the slip rate on the Narlı Fault should be much lower.

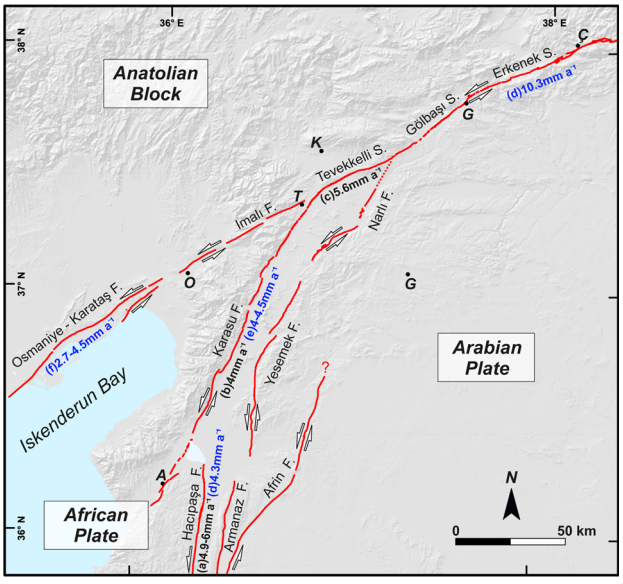



**Fig. 8.** Shaded relief map of southwestern part of EAF (30 m resolution SRTM data), showing the active faults in red. C, Çelikhan; G, Gölbaşı; K, Kahramanmaras; O, Osmaniye; G, Gaziantep; A, Antakya; T, Türkoğlu. Numbers are the slip rates obtained by geological–palaeoseismological studies (black) and GPS studies (blue). Sources for the slip rates: (**a**) Altunel *et al.* (2009), Karabacak *et al.* (2010); (**b**) Karabacak (2007), Rojay *et al.* (2001); (**c**) this study; (**d**) Aktuğ *et al.* (2016); (**e**, **f**) Mahmoud *et al.* (2013), Aktuğ *et al.* (2016).

## Conclusion

We found evidence for at least five and possibly more surface ruptures over the past 10 kyr in our palaeoseismological trenches along the Pazarcık segment of the EAF. We have not identified evidence of the 1513 earthquake in our Balkar trench and we interpret that this event did not generate a surface rupture through the Gölbaşı Basin. The 1513 earthquake rupture most probably was terminated to the NE by the Kartal restraining bend, which represents the most prominent change in the fault trend. The historical 1114 earthquake was recognized at both trench sites in the NE and SW parts of the segment. Considering the extensive damage reported across the Kahramanmaraş region in historical accounts and the rupture observed in the trenches, we suggest that the 1114 earthquake ruptured at least the entire Pazarcık segment and possibly produced a surface rupture of similar length to the 6 February 2023 Pazarcık–Kahramanmaraş earthquake.

Our trench data allow us to infer that the Tevekkelli and Gölbaşı sub-segments were ruptured by different earthquakes in the past that reflect at least two types of rupture behaviour along the EAF segments. Thus the EAF has a similar bimodal behaviour to other continental transform faults.

The slip rate of 5.6 mm $a^{-1}$ over the last 18 kyr obtained from studies of an offset buried stream channel in the southwestern part of the Pazarcık segment is consistent with the slip rate estimate on the main branch of the Dead Sea Fault. A higher slip rate can be considered after the intersection of the Narlı Fault as it accommodates a considerable amount of slip, as was observed after the 6 February 2023 Pazarcık–Kahramanmaraş earthquake. It may be concluded that slip transfer between the EAF and the Dead Sea Fault is provided by faults on both the Karasu and Narlı faults.

*Scientific editing by Matias Ghiglione*

**Acknowledgements** The first fieldwork for this study was conducted between 2009 and 2012. It was completed in February 2023 with coseismic surface rupture observations and offset measurements of the Pazarcık (Kahramanmaraş) Earthquake. We would like to thank Prof. Erhan Altunel for his guidance during the first study. We would like to express our gratitude to I. Gümüş and S. Altınok Erayık, who assisted in the field. We are grateful to V. H. Garcia and G. De Pascale for constructive feedback on the paper.

**Author contributions** **ÖY**: conceptualization (equal), formal analysis (equal), investigation (equal), methodology (equal), writing – original draft (equal), writing – review & editing (equal); **VK**: conceptualization (equal), formal analysis (equal), investigation (equal), methodology (equal), writing – original draft (equal), writing – review & editing (equal)

**Funding** This study has been funded by the Scientific and Technological Research Council of Turkey (TÜBİTAK) as project 109Y043 (co-ordinated by V.K.). A major part of this paper was part of Ö.Y.'s PhD thesis, completed at Eskişehir Osmangazi University in 2012 under the supervision of E. Altunel, with a scholarship from the TÜBİTAK project (109Y043).

**Competing interests** The authors declare that they have no known competing financial interests or personal relationships that could have appeared to influence the work reported in this paper.

**Data availability** All data generated or analysed during this study are included in this published article and its supplementary information file.

## References

Abdalyan, S. 1935. Etude sur le violent tremblement de terre de Zanguezurr en Arménie soviétique. *Revue de Géographie Physique et de Géologie Dynamique*, **1935**, 51–101.

Aksoy, E., İnceöz, M. and Koçyiğit, A. 2007. Lake Hazar Basin: a negative flower structure on the East Anatolian Fault System (EAFS), SE Turkey. *Turkish Journal of Earth Sciences*, **16**, 319–338.

Aktuğ, B., Özener, H. *et al.* 2016. Slip rates and seismic potential on the East Anatolian Fault System using an improved GPS velocity field. *Journal of Geodynamics*, **94–95**, https://doi.org/10.1016/j.jog.2016.01.001

Allen, C.R. 1969. *Active faulting in northern Turkey*. Contribution 1577, Division of Geological Sciences, California Institute of Technology.

Altunel, E., Meghraoui, M., Karabacak, V., Akyuz, H.S., Ferry, M., Yalciner, C.C. and Munschy, M. 2009. Archeological sites (Tell and Road) offset by the Dead Sea Fault in the Amik Basin, Southern Turkey. *Geophysical Journal International*, **179**, https://doi.org/10.1111/j.1365-246X.2009.04388

Ambraseys, N.N. 1989. Temporary seismic quiescence: SE Turkey. *Geophysical Journal International*, **96**, 311–331, https://doi.org/10.1111/j.1365-246X.1989.tb04453.x

Ambraseys, N.N. and Jackson, J.A. 1998. Faulting associated with historical and recent earthquakes in the Eastern Mediterranean region. *Geophysical Journal International*, **133**, 390–406, https://doi.org/10.1046/j.1365-246X.1998.00508.x

Arpat, E. and Şaroğlu, F. 1975. Türkiye'deki bazı önemli genç tektonik olaylar. *TJK Bülteni*, **18**, 91–101.

Arvanitakis, G.L. 1903. Essai d'une statistique des tremblements de terre en Palestine et Syrie. *Bulletin de l'Institut Egyptien*, **4**, Série 4, 178–183.

Barka, A. and Kadinsky-Cade, K. 1988. Strike-slip fault geometry in Turkey and its influence on earthquake activity. *Tectonics*, **7**, 663–684, https://doi.org/10.1029/TC007i003p00663

Ben-Manahem, A. 1979. Earthquake catalogue for the Middle East (92 B.C.–1980 A.D.). *Bollettino di Geofisica Teorica ed Applicate*, **XXIN**, 81.

Bertrand, S. 2006. *Tectonique active à la jonction des plaques Africa, Arabie et Anatolie–Eurasie (sud de la Turquie): caractérisation des failles et analyse de la déformation par un réseau GPS dense*. PhD thesis, Institut de Physique du Globe de Strasbourg.

Bronk Ramsey, C. 2017. Methods for summarizing radiocarbon data-sets. *Radiocarbon*, **59**, 1809–1833, https://doi.org/10.1017/RDC.2017.108

Calvi, W.S. 1941. *Erdbebenkatalog der Turkei und Einiger Benachbarter Gebiete*. MTA (General Directorate of Mineral Research and Exploration), Report, Ankara [in German].

Cavalié, O. and Jónsson, S. 2014. Block-like plate movements in eastern Anatolia observed by InSAR. *Geophysical Research Letters*, **41**, 26–31, https://doi.org/10.1002/2013GL058170

Çetin, H., Güneyli, H. and Mayer, L. 2003. Paleoseismology of the Palu–Lake Hazar segment of the East Anatolian Fault Zone, Turkey. *Tectonophysics*, **374**, 163–197, https://doi.org/10.1016/j.tecto.2003.08.003

De Pascale, G.P., Quigley, M.C. and Davies, T.R. 2014. Lidar reveals uniform Alpine Fault offsets and bimodal plate boundary rupture behavior, New Zealand. *Geology*, **42**, 411–414, https://doi.org/10.1130/G35100.1

Dewey, J.F., Pitman, W.C., III, Ryan, W.B.F. and Bonnin, J. 1973. Plate tectonics and the evolution of the Alpine System. *GSA Bulletin*, **84**, 3137–3180, https://doi.org/10.1130/0016-7606(1973)84%3C3137:PTATEO%3E2.0.CO;2

Duman, T.Y. and Emre, Ö. 2013. The East Anatolian Fault: geometry, segmentation and jog characteristics. *Geological Society, London, Special Publications*, **372**, https://doi.org/10.1144/SP372.14

Emre, Ö., Duman, T.Y., Özalp, S., Elmacı, H., Olgun, Ş. and Şaroğlu, F. 2013. *Active Fault Map of Turkey with an Explanatory Text 1:1,250,000 Scale*. General Directorate of Mineral Research and Exploration, Special Publications, **30**.

Guidoboni, E. and Comastri, A. 2005. *Catalogue of Earthquakes and Tsunamis in the Mediterranean Area from the 11th to the 15th century*. Istituto Nazionale di Geofisica e Vulcanologia.

Hempton, M.R. 1987. Constraints on Arabian plate motion and extensional history of the Red Sea. *Tectonics*, **6**, 687–705, https://doi.org/10.1029/TC006i006p00687

Herece, E. 2008. *Doğu Anadolu Fayı (DAF) Atlası*. General Directorate of Mineral Research and Exploration, Special Publications, **13**.

Jackson, J. and McKenzie, D. 1984. Active tectonics of the Alpine–Himalayan belt between western Turkey and Pakistan. *Geophysical Journal of the Royal Astronomical Society*, **77**, 185–264, https://doi.org/10.1111/j.1365-246X.1984.tb01931.x

Karabacak, V. 2007. *Quaternary Activity of the Northern Dead Sea Fault Zone*. PhD thesis, Eskisehir Osmangazi University, Natural and Applied Sciences Institute [in Turkish with English abstract].

Karabacak, V., Altunel, E., Meghraoui, M. and Akyüz, H.S. 2010. Field evidences from northern Dead Sea Fault Zone (South Turkey): new findings for the initiation age and slip rate. *Tectonophysics*, **480**, 172–182, https://doi.org/10.1016/j.tecto.2009.10.001

Karabacak, V., Uysal, I.T. *et al.* 2019. Are U–Th dates correlated with historical records of earthquakes? Constraints from co-seismic carbonate veins within the North Anatolian Fault Zone. *Tectonics*, **38**, 2431–2448, https://doi.org/10.1029/2018TC005450

Karabacak, V., Özkaymak, Ç *et al.* 2023. The 2023 Pazarcık (Kahramanmaraş, Türkiye) earthquake ($M_w$ 7.7): implications for surface rupture dynamics along the East Anatolian Fault Zone. *Journal of the Geological Society, London*, **180**, https://doi.org/10.1144/jgs2023-020

Kasapoğlu, K.E. 1987. Doğu Akdeniz' in sismotektonik özellikleri: sonlu elemanlar çözümlemesi (Seismotectonic characteristics of eastern Mediterranean: a finite element analysis). *Yerbilimleri*, **14**, 309–317.

Kelling, G., Gökçen, S.L., Floyd, P.A. and Gökçen, N. 1987. Neogene tectonics and plate convergence in the Eastern Mediterranean: new data from southern Turkey. *Geology*, **15**, 425–429, https://doi.org/10.1130/0091-7613(1987)15%3C425:NTAPCI%3E2.0.CO;2

Kempler, D. and Garfunkel, Z. 1991. Northeast Mediterranean triple junction from a plate kinematics point of view. *Bulletin of the Technical University of İstanbul*, **44**, 425–454.

Kiratzi, A. 1993. A study on the active crustal deformation of the North and East Anatolian Fault Zones. *Tectonophysics*, **225**, 191–203, https://doi.org/10.1016/0040-1951(93)90279-S

Koçyiğit and Erol 2002 (details to be added to reference list).

Lyberis, N., Tekin, Y., Chorowicz, J., Kasapoğlu, E. and Gündoğdu, N., 1992. The East Anatolian Fault: an oblique collisional belt. *Tectonophysics,* **204**, 1–15, https://doi.org/10.1016/0040-1951(92)90265-8

Mahmoud, Y., Masson, F. *et al.* 2013. Kinematic study at the junction of the East Anatolian fault and the Dead Sea fault from GPS measurements. *Journal of Geodynamics*, **67**, 30–39, https://doi.org/10.1016/j.jog.2012.05.006

McKenzie, D.P. 1970. Plate tectonics of the Mediterranean region. *Nature*, **220**, 239–343, https://doi.org/10.1038/226239a0

McKenzie, D.P. 1972. Active tectonics of the Mediterranean region. *Geophysical Journal of the Royal Astronomical Society*, **30**, 109–185, https://doi.org/10.1111/j.1365-246X.1972.tb02351.x

Över, S., Özden, S. and Yılmaz, H. 2004. Late Cenozoic stress evolution along the Karasu Valley, SE Turkey. *Tectonophysics*, **380**, 43–68, https://doi.org/10.1016/j.tecto.2003.11.011

Reilinger, R., McClusky, S. *et al.* 2006. GPS constraints on continental deformation in the Africa–Arabia–Eurasia continental collision zone and implications for the dynamics of plate interactions. *Journal of Geophysical Research: Solid Earth*, **111**, https://doi.org/10.1029/2005JB004051

Reimer, P.J., Bard, E. *et al.* 2013. IntCal13 and Marine13 radiocarbon age calibration curves 0–50,000 years cal BP. *Radiocarbon*, **55**, 1869–1887, https://doi.org/10.2458/azu_js_rc.55.16947

Rojay, B., Heimann, A. and Toprak, V. 2001. Neotectonic and volcanic characteristics of the Karasu fault zone (Anatolia, Turkey): the transition zone between the Dead Sea transform and the East Anatolian fault zone. *Geodinamica Acta*, **14**, 197–212, https://doi.org/10.1080/09853111.2001.11432444

Şaroğlu, F., Emre, Ö. and Kuşçu, I. 1992. The East Anatolian fault zone of Turkey. *Annales Tectonicae*, **6**, 99–125.

Şengör, A.M.C. 1980. Türkiye'nin neotektoniğinin esasları. *Türkiye Jeoloji Kurumu, Conference Series*, **2**, 40.

Şengör, A.M.C., Görür, N. and Şaroğlu, F. 1985. Strike-slip faulting and related basin formation in zone of tectonic escape: Turkey as a case study. *SEPM Special Publications*, **37**, 227–264.

Seymen, İ. and Aydın, A. 1972. Bingöl deprem fayı ve bunun Kuzey Anadolu Fayı ile ilişkisi. *MTA Bülteni*, **79**, 1–8.

Seyrek, A., Demir, T., Pringle, M.S., Yurtmen, S., Westaway, R.W.C., Beck, A. and Rowbotham, G. 2007. Kinematics of the Amanos Fault, southern Turkey, from Ar/Ar dating of offset Pleistocene basalt flows: transpression between the African and Arabian plates. *Geological Society, London, Special Publications*, **290**, 255–284, https://doi.org/10.1144/SP290.9

Sieberg, A. 1932. Erdbebengeographie. *Handbuch der Geophysik*, **4**, 775–812.

Soysal, H., Sipahioğlu, S., Kolçak, D. and Altınok, Y. 1981. *Earthquake Catalogue of Turkey and Surroundings, BC 2100–AD 1900*. TUBITAK (Scientific & Technological Research Council of Turkey) Research Project, Final Report (Project TBAG 341).

Taymaz, T., Eyidoğan, H. and Jackson, J. 1991. Source parameters of large earthquakes in the EAF (Turkey). *Geophysical Journal International*, **106**, 537–550, https://doi.org/10.1111/j.1365-246X.1991.tb06328.x

Walters, R.J. 2013. *Geodetic Observation and Modelling of Continental Deformation in Iran and Turkey*. DPhil thesis, University of Oxford.

Westaway, R. and Arger, J. 1996. The Gölbaşı basin, southeastern Turkey: a complex discontinuity in a major strike-slip fault zone. *Geophysical Journal International*, **153**, 729–743.

Yönlü, Ö, Altunel, E., Meghraoui, M., Karabacak, V., Ferry, M., Yalciner, C.C. and Kıyak, N. 2010. Paleoseismological evidences about the long term activity of the northernmost Dead Sea Fault Zone, Turkey. 7th International Symposium on Eastern Mediterranean Geology, 18–22 October 2010. University of Cukurova, Adana, Turkey.

Yönlü, Ö, Altunel, E., Karabacak, V. and Akyuz, H.S. 2013. Evolution of the Golbasi Basin and its implications for the long-term offset of the East Anatolian Fault Zone, Turkey. *Journal of Geodynamics*, **65**, https://doi.org/10.1016/j.jog.2012.04.013

Yönlü, Ö, Altunel, E. and Karabacak, V. 2017. Geological and geomorphological evidence for the southwestern extension of the East Anatolian Fault Zone, Turkey. *Earth and Planetary Science Letters*, **469**, 1–14, http://doi.org/10.1016/j.epsl.2017.03.034

Yürür, M.T. and Chorowicz, J. 1998. Recent volcanism, tectonics and plate kinematics near the junction of the African, Arabian and Anatolian plates in the Eastern Mediterranean. *Journal of Volcanology and Geothermal Research*, **85**, 1–15, https://doi.org/10.1016/S0377-0273(98)00046-8

Zielke, O., Arrowsmith, J.R., Ludwig, L.G. and Akciz, S.O. 2010. Slip in the 1857 and earlier large earthquakes along the Carrizo Plain, San Andreas fault. *Science*, **327**, 1119–1122, https://doi.org/10.1126/science.1182781

View publication stats